ISSN 1674-1056
http://cpb.iphy.ac.cn
http://iopscience.iop.org/cpb
中国物理 B
Chinese Physics
中国物理
Chinese Physics B

Structural phase transition, strength, and texture in vanadium at high pressure under nonhydrostatic compression

Lun Xiong(熊伦), Jing Liu(刘景)
Citation: Chin. Phys. B . 2018, 27(3): 036101. **doi:** 10.1088/1674-1056/27/3/036101

Journal homepage: http://cpb.iphy.ac.cn; http://iopscience.iop.org/cpb

What follows is a list of articles you may be interested in

High pressure structural phase transitions of TiO_2 nanomaterials

Quan-Jun Li(李全军), Bing-Bing Liu(刘冰冰)
Chin. Phys. B . 2016, 25(7): 076107. **doi:** 10.1088/1674-1056/25/7/076107

Behaviors of Zn_2GeO_4 under high pressure and high temperature

Shu-Wen Yang(杨淑雯), Fang Peng(彭放), Wen-Tao Li(李文涛), Qi-Wei Hu(胡启威), Xiao-Zhi Yan(晏小智), Li Lei(雷力), Xiao-Dong Li(李晓东), Duan-Wei He(贺端威)
Chin. Phys. B . 2016, 25(7): 076101. **doi:** 10.1088/1674-1056/25/7/076101

Phase transition and chemical decomposition of liquid carbon dioxide and nitrogen mixture under extreme conditions

Xiao-Xu Jiang(姜晓旭), Guan-Yu Chen(陈冠宇), Yu-Tong Li(李玉同), Xin-Lu Cheng(程新路), Cui-Ming Tang(唐翠明)
Chin. Phys. B . 2016, 25(2): 026102. **doi:** 10.1088/1674-1056/25/2/026102

Li-ion batteries: Phase transition

Peiyu Hou(侯配玉), Geng Chu(褚赓), Jian Gao(高健), Yantao Zhang(张彦涛), Lianqi Zhang(张联齐)
Chin. Phys. B . 2016, 25(1): 016104. **doi:** 10.1088/1674-1056/25/1/016104

Anomalous phase transition of InN nanowires under high pressure

Tang Shun-Xi, Zhu Hong-Yang, Jiang Jun-Ru, Wu Xiao-Xin, Dong Yun-Xuan, Zhang Jian, Yang Da-Peng, Cui Qi-Liang
Chin. Phys. B . 2015, 24(9): 096101. **doi:** 10.1088/1674-1056/24/9/096101

Structural phase transition, strength, and texture in vanadium at high pressure under nonhydrostatic compression*

Lun Xiong(熊伦)[1,2,3,†] and Jing Liu(刘景)[3]

[1] School of Intelligent Manufacturing, Sichuan University of Arts and Science, Dazhou 635000, China
[2] DaZhou Industrial Technology Institute of Intelligent Manufacturing, Dazhou 635000, China
[3] Beijing Synchrotron Radiation Facility, Institute of High Energy Physics, Chinese Academy of Sciences, Beijing 100049, China

(Received 29 September 2017; revised manuscript received 23 December 2017; published online 11 February 2018)

The structural phase transition, strength, and texture of vanadium have been studied under nonhydrostatic compression up to 70 GPa using an angle-dispersive radial x-ray diffraction technique in a 2-fold paranomic diamond anvil cell and up to 38 GPa using an angle-dispersive x-ray diffraction technique in a modified Mao–Bell diamond anvil cell at room temperature. We have confirmed a phase transition from body-centered cubic structure to rhombohedral structure at 27–32 GPa under nonhydrostatic compression. The radial x-ray diffraction data yields a bulk modulus $K_0 = 141(5)$ GPa and its pressure derivative $K_0' = 5.4(7)$ for the bcc phase and $K_0 = 154(13)$ GPa with $K_0' = 3.8(3)$ for the rhombohedral phase at $\psi = 54.7°$. The nonhydrostatic x-ray diffraction data of both bcc and rhombohedral phases yields a bulk modulus $K_0 = 188(5)$ GPa with $K_0' = 2.1(3)$. Combined with the independent constraints on the high-pressure shear modulus, it is found that the vanadium sample can support a differential stress of ~1.6 GPa when it starts to yield with plastic deformation at ~36 GPa. A maximum differential stress as high as ~ 1.7 GPa can be supported by vanadium at the pressure of ~ 47 GPa. In addition, we have investigated the texture up to 70 GPa using the software package MAUD. It is convinced that the body-centered cubic to rhombohedral phase transition and plastic deformation due to stress under high pressures are responsible for the development of texture.

Keywords: phase transition, strength, texture, vanadium

PACS: 61.05.cp, 62.20.F–, 07.35.+k, 64.30.Ef **DOI:** 10.1088/1674-1056/27/3/036101

1. Introduction

Vanadium (V) is a transition metal with body-centered cubic (bcc) structure under ambient conditions and its superconducting critical temperature T_c is the subject of previous reports.[1–4] Later, the high-pressure structure of pure crystalline V was the focus of an intense research effort.[5–7] Takemura *et al.*[5] performed high-pressure diamond anvil cell (DAC) powder x-ray diffraction (XRD) experiments on V under hydrostatic conditions and reported that the body-centered cubic (bcc) phase remained stable up to the maximum pressure of 154 GPa. Suzuki and Otani[6] calculated the lattice dynamics of the bcc phase of V in the pressure range up to 150 GPa using the first-principles theory. The authors found that a remarkable anomaly of phonon occurred at pressures higher than 130 GPa, indicating the possibility of a structural phase transition. Subsequently, Landa *et al.*[7] calculated the equation of state (EOS) and shear elastic constants of bcc V as a function of pressure up to 600 GPa using first principles. The authors found that pressure-induced shear elastic constant anomalies (softening) appeared at ~ 200 GPa, suggesting the possibility of a structural transition from bcc to another phase.

As far as the theoretical calculation was concerned,[6,7] the early works raised a renewed interest in the phase transition of V. Subsequently, Ding *et al.*[8] revealed a phase transition characterized by a rhombohedral lattice distortion in the bcc lattice at ~ 69 GPa at room temperature in V using synchrotron x-ray diffraction technique in a DAC. The author reported that the rhombohedral phase was stable up to the highest pressure of 155 GPa. In addition, they interpreted this phase transition as a second-order transition, because the transition was not accompanied by any jump of the volume with increasing pressure. This form of transition has never been reported in any other transition metal or other pure elements, thus represents an entirely different trend from the previous ones.

Later on, the possibility of the rhombohedral phase in V under pressure was confirmed by first-principles calculations.[9–13] Lee *et al.*[9] calculated the transition pressure as 84 GPa and firstly discovered a re-entrant bcc phase at ultrahigh pressures above 280 GPa. Luo *et al.*[10] confirmed that the first phase transition occurring at ~ 62 GPa was derived by phonon softening from bcc to hR1, and the authors firstly predicted two new phase transitions: one from hR1 (110.5°) to distorted-hR1 (108.2°) at ~ 120 GPa, and finally the re-entrance of the bcc phase at ~ 250 GPa, which became

*Project supported by the National Natural Science Foundation of China (Grant Nos. 10875142 and 11079040) the Project of Sichuan University of Arts and Science, China (Grant No. 2017KZ001Z), and the Program of Education Department of Sichuan Province, China (Grant No. 18ZB0506). This work was performed at 4W2 beamline of Beijing Synchrotron Radiation Facility (BSRF), which was supported by Chinese Academy of Sciences (Grant Nos. KJCX2-SWN03 and KJCX2-SW-N20).

†Corresponding author. E-mail: 1094129778@qq.com

© 2018 Chinese Physical Society and IOP Publishing Ltd

stable again up to the highest pressure of 400 GPa. Koči *et al.*[11] demonstrated that the elastic constant softening in V arising from the Fermi surface nesting was responsible for the bcc→rhombohedral transition at 80 GPa. Qiu and Marcus[12] firstly reported one bcc→rh^{u} (rhombohedral phase) transition identified as a thermodynamic transition (not observed in the previous experiment) at 32 GPa, and the other at 65 GPa as an instability transition when the bcc phase became unstable (observed in the previous experiment). In addition, the transition rh^{u} →rh^{l} (the other rhombohedral phase) appeared at 115 GPa is a thermodynamic transition and an instability transition, and the transition rh^{l} →bcc at 297 GPa is identified as a thermodynamic transition. Subsequently, the structural phase transition sequence was confirmed by Verma *et al.*[13] as bcc (60 GPa)→Rhom1 ($\alpha = 110.50°$, 160 GPa)→Rhom2 ($\alpha = 108.50°$, 240 GPa)→bcc.

More recently, whether the transition from bcc to rhombohedral phase in V is a second-order transition has been extensively discussed by first-principles calculations.[14–17] Lee *et al.*[14] reported that the volume change associated with these transitions was less than 0.15%, but the transitions were first order, as calculations of the single crystal and polycrystal elastic moduli (stress–strain) coefficients revealed a small discontinuity in the shear modulus and other elastic properties across the phase transition. Krasil'nikov *et al.*[15–17] calculated the second- and third-order Brugger constants based on the Landau theory, and demonstrated that the phase transition observed in V at the pressure of 69 GPa was a first-order elastic phase transition close to a second-order one.

Recently, Jenei *et al.*[18] found that the bcc to rhombohedral phase transition occurred at 30 GPa at room temperature and 37 GPa at 425 K under the nonhydrostatic condition. The transition pressure of 30 GPa obtained by Jenei *et al.*[18] is much lower than the value of 69 GPa previously reported by Ding *et al.*[8] under nonhydrostatic compression at room temperature. In the experimental reports on compressibility of V,[8,18] the previous results present a large discrepancy of transition pressure as high as 39 GPa. Thus, it is of great importance to confirm the bcc-to-rhombohedral transition pressure.

In the present work, we investigate the V sample under nonhydrostatic compression using angle dispersive x-ray diffraction (ADXRD) technique in a radial diamond anvil cell (rDAC) and ADXRD technique in a modified Mao–Bell DAC. Combined with the lattice strain theory,[19,20] the structural phase transition, strength, and texture of V up to 70 GPa are obtained.

2. Experimental details

For the radial x-ray diffraction (RXRD) measurements, a 2-fold paranomic DAC with 300 μm culet diameter was used to exert uniaxial compression on the V sample. A beryllium (Be) gasket was pre-indented to ∼ 25-μm thick at ∼ 20 GPa. The V sample (−325 mesh, with a purity of 99.5% from Alfa Aesar) was loaded into a 60-μm-diameter hole in the Be gasket for RXRD measurements. A ruby chip with a diameter of ∼ 10 μm served as the pressure standard.[21] No pressure-transmitting medium was used to ensure maximum nonhydrostatic stresses. The DAC was tilted to an angle of 28° to minimize the contribution of Be diffraction lines to the sample patterns.[22]

For the nonhydrostatic ADXRD experiments, we used a modified Mao–Bell DAC with 300 μm culet diameter. A T301 gasket was pre-indented to ∼ 30 μm thick and a 100 μm diameter hole was drilled at the center of the gasket. Powder V sample was loaded in the sample chamber without a pressure medium. A ∼ 10 μm ruby chip was used as a pressure sensor[21] and placed on top of the sample center.

The *in situ* high-pressure RXRD experiments were conducted at the 4W2 beam line of Beijing Synchrotron Radiation Facility (BSRF) with a wavelength of 0.6199 Å and the x-ray beam was focused to the size of 30 μm×8 μm (FWHM) using Kirkpatrick–Baez mirrors. The power diffraction patterns were collected with a Mar345 image plate and integrated with the Fit2D[23] software package. At each pressure, the RXRD pattern was collected for 20 min after ∼ 30 min stress relaxation.

3. Theory

The RXRD data was analyzed using the lattice strain theory developed by Singh *et al.*[19,20] The measured d-spacing $d_{\mathrm{m}}(hkl)$ is a function of the azimuthal angle ψ (between the DAC loading axis and the diffraction plane normal hkl), and can be calculated as

$$d_{\mathrm{m}}(hkl) = d_p(hkl)[1 + (1 - 3\cos^2\psi)Q(hkl)], \qquad (1)$$

where $d_{\mathrm{m}}(hkl)$ is the measured d spacing, and $d_p(hkl)$ is the d spacing under the equivalent hydrostatic pressure. $Q(hkl)$ is the orientation-dependent lattice strain, and can be expressed as the harmonic mean of the aggregate x-ray shear moduli under assumptions of stress continuity and strain continuity. ψ in Eq. (1) can be rewritten as[24]

$$\cos\psi_{hkl} = \sin\beta\cos\delta\cos\theta_{hkl} + \cos\beta\sin\theta_{hkl}, \qquad (2)$$

where θ is the diffraction angle, δ is the azimuthal angle in the plane of the detector, and β equals 28°. $Q(hkl)$ can be expressed as

$$Q(hkl) = (t/3)\left\{\alpha[2G_{\mathrm{R}}^{\mathrm{X}}(hkl)]^{-1} + (1-\alpha)(2G_{\mathrm{V}})^{-1}\right\}, \qquad (3)$$

where G is the termed shear modulus, and the subscripts R and V denote Reuss (stress continuity) and Voigt (strain continuity) assumptions, respectively. The superscript X denotes the average relevant to XRD. α determines the relative weights

of the Reuss and Voigt terms. In most high-pressure experiments, satisfactory interpretations of the data have been made with $\alpha = 1$, and the following relation can be derived:

$$t = 6G\langle Q(hkl)\rangle, \tag{4}$$

where $\langle Q(hkl)\rangle$ represents the average $Q(hkl)$ over (hkl). G is the aggregate shear modulus of the polycrystalline aggregate. The pressure dependence of G can be obtained from the extrapolation of ultrasonic or theoretically calculated single-crystal elastic constant. If the differential stress has reached its limiting value of yield strength at high pressures, t/G will reflect the ratio of yield strength to shear modulus.[25,26]

4. Results and discussion

The program Multifit 4.2[24] was used to yield one-dimensional plots of the x-ray intensity as a function of 2θ and fit peak positions. We used this software package to fit peak positions with segments of 5° intervals in the azimuth angle, in steps from 90° to 180°. RXRD spectra of V were collected up to 70 GPa, where the pressures were derived from the ruby chip.[21] The selected 2θ–intensity diffraction patterns of the sample taken at $\psi_{hkl} = 54.7°$ under different pressures are shown in Fig. 1(a). Five diffraction peaks (110, 200, 211, 220, 310) of the bcc phase were observed at low pressures. During the transition from the bcc to rhombohedral structure at 27 GPa, the cubic (110) diffraction peak split into rhombohedral (−110) and (100) peaks (see Fig. 1(b)), the cubic (211) peak split into rhombohedral (−211), (−210) and (110) peaks, the cubic (220) split into rhombohedral (−220) and (200) peaks, and the cubic (310) peak split into rhombohedral (−221) and (21 − 1) peaks. In spite of the transition from the bcc to rhombohedral phase, the cubic (200) peak and the rhombohedral (−111) peak remained as a single sharp peak up to our maximum pressure of 70 GPa.

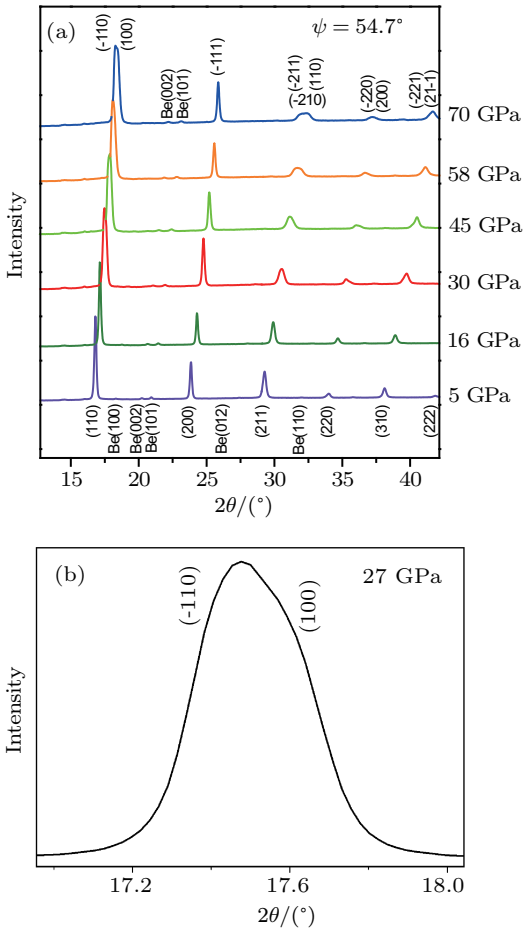


Fig. 1. (color online) (a) Selected diffraction patterns of V under nonhydrostatic compression taken at $\psi = 54.7°$. (b) The cubic (110) diffraction peak splits into rhombohedral (−110) and (100) peaks during the transition from the bcc to rhombohedral structure at 27 GPa.

The nonhydrostatic ADXRD experiments were carried out up to 38 GPa, and V remained in the bcc structure until the (110) and (211) peaks split above 32 GPa. The (200) diffraction stayed as a single sharp peak up to the maximum pressure (see Fig. 2), thus confirming the phase transition from the cubic to rhombohedral lattice.

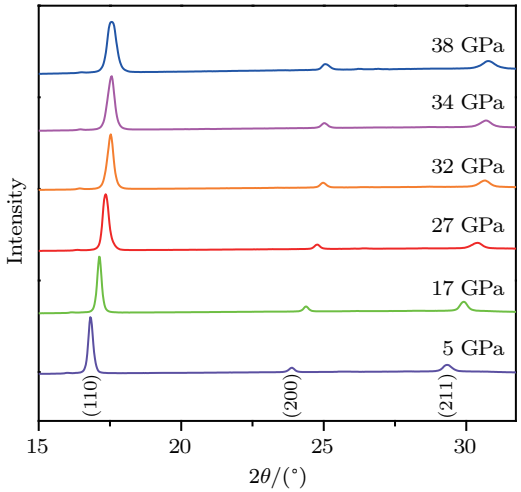


Fig. 2. (color online) Nonhydrostatic XRD of V at selected pressures.

4.1. Estimation of transition pressure

The rhombohedral structure can be described by a one-atom unit cell with $a = b = c$ and $\alpha = \beta = \gamma$. The one-atom bcc unit cell can be represented as a special case of the 1-atom rhombohedral unit cell with $a = \sqrt{3}/2a_0$ and $\alpha = 109.47°$, where a_0 is the lattice constant of the conventional cubic 2-atom bcc cell.[12] The volume of the rhombohedral unit cell is given by $V = a^3(1 - \cos\alpha)\sqrt{1 + 2\cos\alpha}$. The transformation from the bcc structure (Im-$3m$) to the rhombohedral structure (R-$3m$) is illustrated in Fig. 3. The phase transition from the bcc to rhombohedral structure at high pressures corresponds to a displacive distortion of the bcc structure along the body diagonal [111] on the $\boldsymbol{a}_1 \times \boldsymbol{a}_2$ plane.

A summary of the transition pressures obtained from the experiments and theoretical calculations is given in Table 1. Our transition pressures of 27 GPa and 32 GPa under nonhydrostatic compression are consistent with the experimental

value of 30 GPa obtained by Jenei *et al.*[18] and the theoretical value of 30 GPa reported by Qiu *et al.*,[12] but much lower than that of 69 GPa reported by Ding *et al.*[8] under nonhydrostatic compression and other theoretical values.[9–11,13] Jenei *et al.*[8] reported the transition pressures of 53 GPa, 63 GPa, and 65 GPa in their quasihydrostatic experiments on V samples using different pressure media of Ar, Ne, and He, respectively. From Ar to He, the quasihydrostatic condition becomes better at high pressures and the transition pressure becomes higher accordingly. In conclusion, the transition under the hydrostatic condition is significantly hindered and it can occur at much lower pressure under the nonhydrostatic condition compared with the ideal hydrostatic conditions. Nonhydrostatic conditions could provide the mechanical mechanism to overcome the energy barriers of the transition and the stress induced in the sample by the pressure gradients due to nonhydrostatic compression. In addition, Jenei *et al.*[8] confirmed the transition pressure of 37(2) GPa at temperature 425 K compared to that of 30 GPa at room temperature. The transition pressure at high temperature is higher than that at room temperature, as the high temperature can reduce the influence due to uniaxial stress.

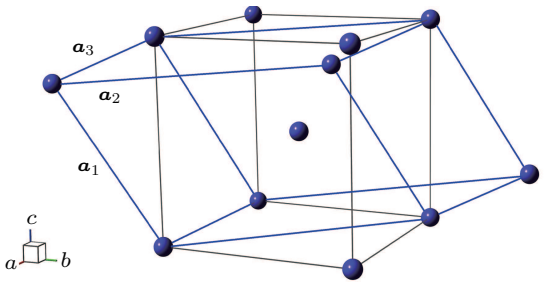


Fig. 3. (color online) The transition from the bcc structure (*Im*-3*m*) to a rhombohedral structure (*R*-3*m*). The bcc unit cell is depicted by the black lines. The rhombohedral unit cell is framed with basis vectors $\boldsymbol{a}_1$, $\boldsymbol{a}_2$, and $\boldsymbol{a}_3$, corresponding to the vectors in the [11-1], [-110], and [111] directions, respectively.

Table 1. A summary of the transition pressure obtained from various methods. PTM refers to pressure-transmitting medium; and R. T. refers to room temperature.

Transition pressure/GPa	Method	PTM	Temperature	Reference
27	RXRD	null	R.T.	Present work
32	XRD	null	R.T.	
69	XRD	null	R.T.	Ding *et al.*[8]
63	XRD	heon	R.T.	
37	XRD	null	425 K	Jenei *et al.*[18]
30	XRD	null	R.T.	
53	XRD	argon	R.T.	
62	XRD	neon	R.T.	
65	XRD	helium	R.T.	
84	theory	–	–	Lee *et al.*[9]
62	theory	–	–	Luo *et al.*[10]
80	theory	–	–	Koci *et al.*[11]
30	theory	–	–	Qiu *et al.*[12]
60	theory	–	–	Verma *et al.*[13]
80	theory	–	–	Lee *et al.*[14]

4.2. Hydrostatic equation of state

The $d_m(hkl)$ vs. $(1-3\cos^2\psi)$ results in the variation are shown in Fig. 4. As expected from the lattice strain theory,[19,20] the measured d-spacings vary linearly with $1-3\cos^2\psi$.

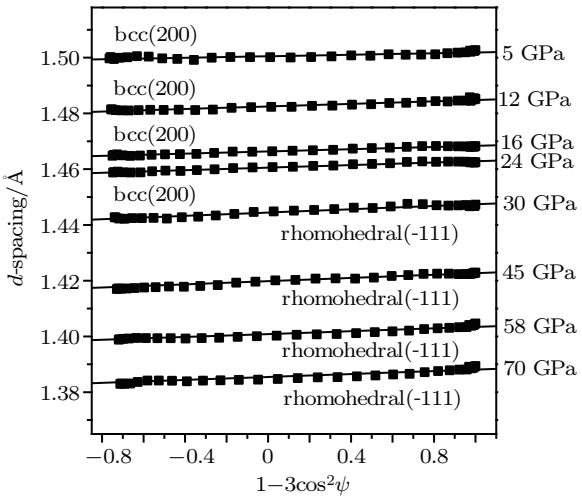


Fig. 4. Dependence of observed d-spacing on $1-3\cos^2\psi$ for the (200) peak of bcc phase and (-111) peak of rhombohedral phase diffraction lines at different pressures. The solid lines are least-squares fits to the data.

For the angle-dispersive RXRD experiments, the d-spacings of $d_p(110)$, $d_p(200)$, $d_p(211)$, $d_p(220)$, and $d_p(310)$ were determined at $\psi = 54.7°$, and were used to calculate the lattice parameter a as well as the equivalent unit cell volume of the bcc phase. For the rhombohedral phase, the lattice parameter a_R and angle α could be calculated from the splitting of the cubic (110), (211), (220), and (310) diffraction lines. At the pressure of 45 GPa, we obtained rhombohedral unit cell parameters $a_R = 2.4649(41)$ Å and $\alpha = 109.61(2)°$.

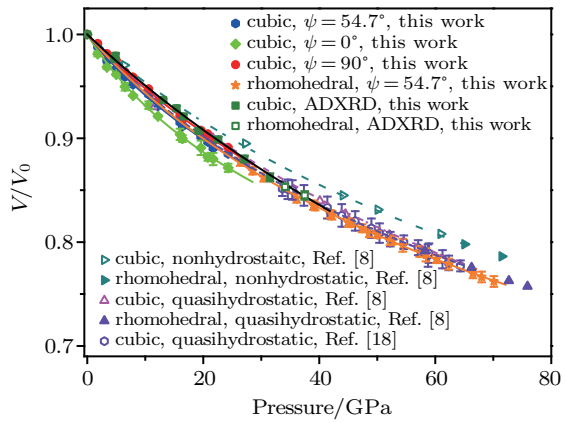


Fig. 5. (color online) Compression curves of V from lattice parameters measured at 0°, 54.7°, and 90°. The solid lines are Birch–Murnaghan equation fitting lines to the data at each angle. Other reported compression data of V are also shown for comparison. The solid right triangles, solid up triangles, open right triangles, and open up triangles are the static compression data from Ref. [8]. The open hexagons are the static compression data obtained by Jenei *et al.*[18]

For the nonhydrostatic ADXRD experiments, we obtained a rhombohedral unit cell of $a_R = 2.4962(63)$ with

$\alpha = 109.63(25)^\circ$ at the transition pressure of 32 GPa. The values of α are in agreement with those reported in previous experiments,[8,18] while slightly smaller than the theoretically calculated values ($\sim 110.25^\circ$).[9–14]

The normalized unit cell volumes of compression curves for $\psi = 0^\circ$, $\psi = 54.7^\circ$, and $\psi = 90^\circ$ are shown in Fig. 5. For comparison, the results obtained in the earlier reports are also included.[8,18]

Fitting the *P*–*V* data with the third-order Birch–Murnaghan equation of state (EOS),[27] we obtained the K_0 and K_0'. For the bcc phase of RXRD data, we obtained the bulk modulus $K_0 = 141(5)$ GPa and its pressure derivative $K_0' = 5.4(7)$ at $\psi = 54.7^\circ$. The bulk moduli obtained from the fitting of the diffraction data at $\psi = 0^\circ$ and 90° were 109(4) GPa and 172(6) GPa, respectively. For the rhombohedral phase, the RXRD data yielded a bulk modulus of $K_0 = 154(13)$ GPa with $K_0' = 3.8(3)$. In addition, we fitted the bcc and rhombohedral phases and obtained the bulk modulus and its pressure derivative as $K_0 = 153(1)$ GPa and $K_0' = 3.9(1)$, respectively. It can be seen that the bulk modulus of the rhombohedral phase is close to that of the two phases. In addition, we classified the phase transition into a second-order or subtle first-order phase transition, as the pressure–volume plot of the two phases displayed no striking discontinuity in the entire pressure range. For comparison, the bulk modulus obtained from the nonhydrostatic ADXRD experiments was $K_0 = 188(5)$ GPa with $K_0' = 2.1(3)$ for the bcc and rhombohedral phases.

A comparison between our research results and the previously reported results[5–11,18] on the bulk modulus (K_0) and its pressure derivative (K_0') is shown in Table 2. It can be seen that the bulk modulus of the bcc phase derived from $\psi = 54.7^\circ$ is consistent with that obtained from x-ray diffraction under quasi-hydrostatic compression obtained by Takemura *et al.*[5] and Ding *et al.*[8] within the experimental error. However, the bulk modulus derived at $\psi = 90^\circ$ of the bcc phase is lower than that obtained by Ding *et al.*[8] under nonhydrostatic compression and Jenei *et al.*[18] under quasihydrostatic compression as well as those obtained by the latest theoretical calculations.[9–14] For the rhombohedral phase, the bulk modulus derived from $\psi = 54.7^\circ$ is much lower than that reported by Jenei *et al.*[18] fitting a Vinet-form universal EOS of both the bcc and rhombohedral phases. In addition, the bulk modulus of both phases obtained from nonhydrostatic ADXRD data without pressure medium is in agreement with the values obtained by Ding *et al.*[8] under nonhydrostatic compression and Jenei *et al.*[18] under quasihydrostatic compression as well as those obtained by the latest theoretical calculations,[9–14] but much higher (18.6%) than the value derived from $\psi = 54.7^\circ$ from RXRD data of the present work. The determination of EOS greatly depends on the nonhydrostatic stress. However, due to the solidification of the pressure medium at high pressure, the ideal hydrostatic environment cannot be maintained over 15 GPa.[28,29] In most cases, the nonhydrostatic compression curve yields a bulk modulus higher (10%–20%) than the value obtained from the quasihydrostatic curve at a given pressure.[30] The advantage of RXRD is that the EOS under equivalent hydrostatic environment can be derived from the data of highly nonhydrostatic compression without any pressure medium, so that the limitation of solidification of pressure medium at high pressure can be overcome.

Table 2. A summary of the bulk modulus K_0 of V and its pressure derivative K_0' obtained from various methods. PTM refers to pressure-transmitting medium; GGA refers to the generalized gradient approximation; DFP refers to density-functional perturbation; GCECEFT refers to gradient-corrected exchange and correlation energy functional theory; EMTO refers to exact muffin-tin orbital; LR-FPLMTO refers to linear-response full-potential linear-muffin-tin-orbital.

K_0/GPa	K_0'	Structure	Method and PTM	Reference
141(5)	5.4(0.7)	bcc	RXRD ($\psi = 54.7^\circ$), null	this work
109(4)	7.1(0.8)	bcc	RXRD ($\psi = 0^\circ$), null	
172(6)	3.3(0.7)	bcc	RXRD ($\psi = 90^\circ$), null	
154(13)	3.8(0.3)	rhombohedral	RXRD ($\psi = 54.7^\circ$), null	
153(1)	3.9(0.1)	bcc+rhombohedral	RXRD ($\psi = 54.7^\circ$), null	
188(5)	2.1(3)	bcc+rhombohedral	ADXRD, null	
188	2.4	bcc	XRD, silicone oil	Takemura *et al.*[5]
158(1)	2.4	bcc	XRD, helium	Ding *et al.*[8]
195(3)	3.9(2)	bcc	XRD, null	
179(8)	3.1(1.2)	bcc	XRD, neon	Jenei *et al.*[18]
202(37)	1.7(1.5)	bcc+rhombohedral	XRD, null	
194.6	3.0	bcc	theory (LR-FPLMTO, EMTO)	Suzuki *et al.*[6]
183		bcc	theory (EMTO)	Landa *et al.*[7]
182		bcc	theory (GCECEFT)	Lee *et al.*[9]
178	4.3	bcc	theory (DFP)	Luo *et al.*[10]
183	3.6	rhombohedral	theory (DFP)	
182	3.8	bcc	theory (GGA)	Koci *et al.*[11]

The pressure dependence of the normalized lattice parameter of the two phases compared with the results reported by Ding *et al.*[8] and Jenei *et al.*[18] is shown in Fig. 6. The V sample displays the characteristic of a second-order or subtle first-order phase transition as the pressure dependences of the lattice parameters are continuous, but their slopes are slightly discontinuous within the experimental error.

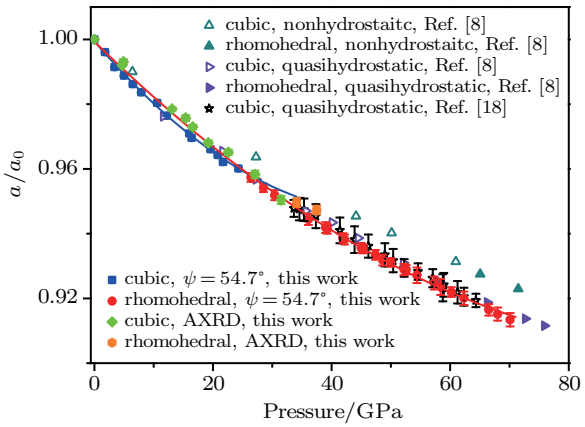


Fig. 6. (color online) Compressibility of the normalized lattice parameters of V compared with the results obtained by Ding *et al.*[8] and Jenei *et al.*[18] The solid lines are quadratic polynomial equation fitting lines to the data.

4.3. Estimation of differential stress

The ratio of differential stress to shear modulus t/G as a function of pressure for V is shown in Fig. 7. It can be seen that the ratio t/G remains constant above 36 GPa, indicating that the V sample starts to suffer yield with plastic deformation at ~ 36 GPa and t/G reaches its limiting value of 0.027 at this pressure. The t/G begins to fall after ~ 49 GPa, suggesting that the local deviatoric stresses start to partially relax.

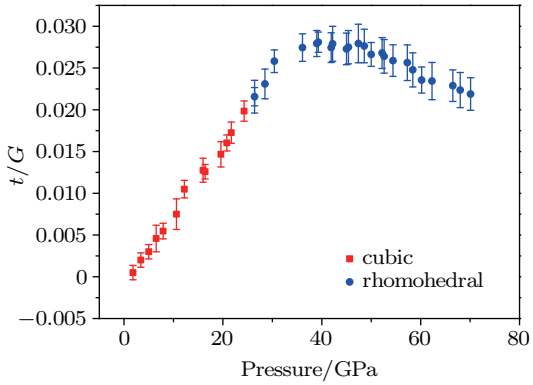


Fig. 7. (color online) Ratio of differential stress to shear modulus (t/G) as a function of pressure for V. The estimated errors are obtained from the scatter of $d(hkl)$ vs. $1-3\cos^2\psi$.

The volume-dependent shear modulus G is expressed as[31]

$$G = G_0(1+2f)^{5/2}\left[1+\left(3K_0\frac{\mathrm{d}G_0}{\mathrm{d}P}/G_0-5\right)f\right], \qquad (5)$$

where $f=[(V_0/V)^{2/3}-1]$, and K_0 and G_0 are the bulk modulus and shear modulus at ambient pressure, respectively. By using the single-crystal elastic modulus of V,[32] the G values at high pressures were derived from Eq. (5).

The relationship between differential stresses and pressure determined from the RXRD experiments of V and the yield strength obtained by Klepeis *et al.*[33] are shown in Fig. 8. In spite of the existence of transition, the differential stress fitting to the data from 2 GPa to 30 GPa yields $t=-0.084(17)+0.050(1)P$ (GPa), where P is the pressure in GPa. The differential stress increases more slowly above ~ 36 GPa, indicating that V starts to suffer from yield at ~ 36 GPa with plastic deformation, and t reaches its limiting value of 1.58 GPa. A maximum differential stress as high as ~ 1.66 GPa can be supported by V at ~ 47 GPa. After ~ 49 GPa, the differential stress begins to fall. In addition, the differential stress in the entire pressure range of the present work is lower than the yield strength obtained by Klepeis *et al.*,[33] indicating the correctness of our results. As $t=\sigma_3-\sigma_1\leq 2\tau=Y$, where τ is the shear strength and Y is the yield strength of the sample.[34]

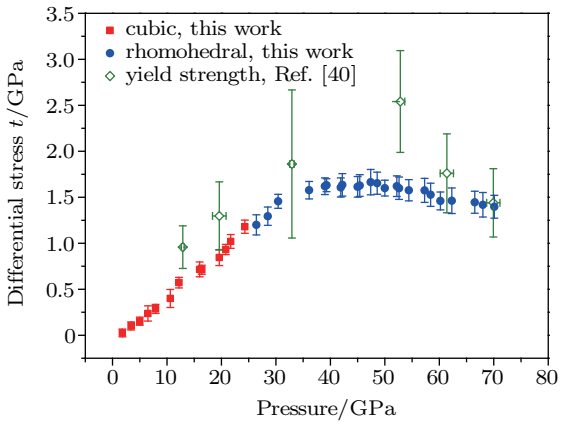


Fig. 8. (color online) Differential stress as a function of pressure for V. The open hexagons are the yield strength as a function of pressure obtained by Klepeis *et al.*[33]

4.4. Estimation of texture

The plastic deformation by dislocation glide generates lattice-preferred orientation (LPO) or texture if the material deforms by slip or mechanical twinning due to plastic deformation. In RXRD geometry, the texture is revealed by variation of intensity along Debye rings and we can extract quantitative texture information using the software package MAUD.[35,36] Figure 9(a) compares the inverse pole figures for 3–24 GPa of the bcc phase. In contrast to typical bcc metals with dominant $\{110\}\langle-111\rangle$ slip,[37] the (001) lattice plane is the most preferred LPO. Interestingly, when the bcc phase transforms to rhombohedral phase under uniaxial stress, it immediately displays a strong texture with a maximum at $\{10\text{-}10\}$ (see Fig. 9(b)). The $\{10\text{-}10\}$ plane of the rhombohedral phase corresponds to (001) lattice planes in the bcc structure. It is determined that the texture is developed by the bcc to rhombohedral phase transition and plastic deformation due to stress under high pressures, as individual crystals deform preferentially on slip planes when the shear stress is applied to polycrystals.[38]

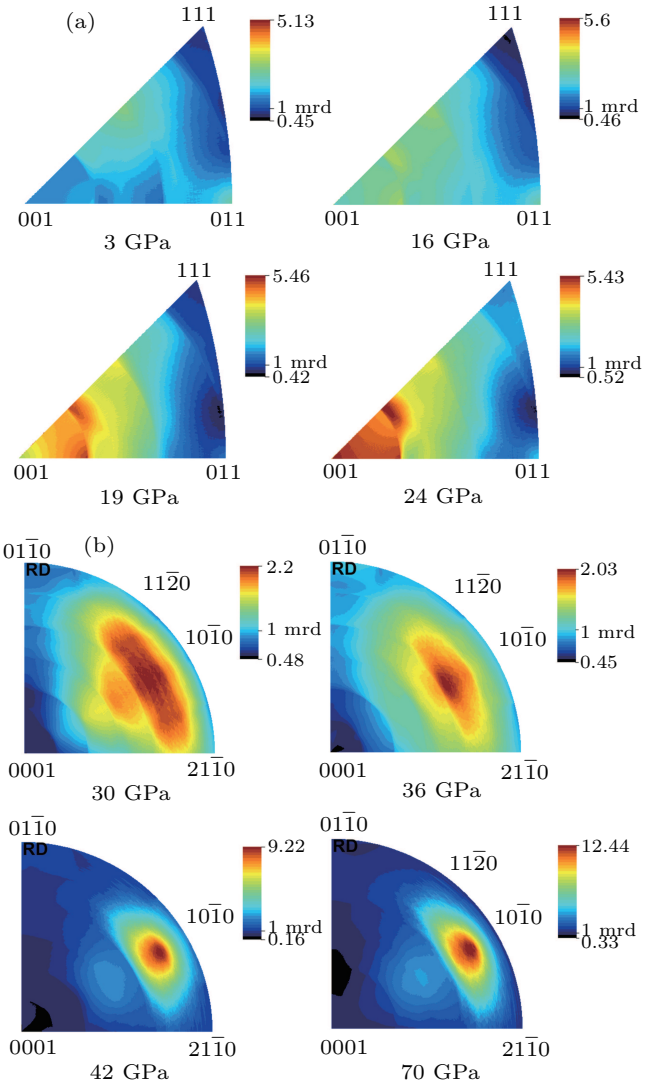


Fig. 9. (color online) Inverse pole figures of V along the compression direction (normal direction) at high pressures. Texture strength is expressed as mrd, where mrd = 1 denotes random distribution, and a higher mrd represents a stronger texture. (a) The bcc phase. (b) The rhombohedral phase.

5. Conclusion

We have examined the structural phase transition, strength, and texture of V up to 70 GPa using RXRD technique and up to 38 GPa using ADXRD technique at room temperature. We are convinced that the phase transition from the bcc to rhombohedral structure occurs at 27–32 GPa. The RXRD data yields a bulk modulus $K_0 = 141(5)$ GPa and its pressure derivative $K_0' = 5.4(7)$ for the bcc phase and $K_0 = 154(13)$ GPa with $K_0' = 3.8(3)$ for the rhombohedral phase at $\psi = 54.7°$. Moreover, the nonhydrostatic ADXRD data yields a bulk modulus $K_0 = 188(5)$ GPa with $K_0' = 2.1(3)$ for both phases. The transition is classified to a second-order or subtle first-order one in the present work as the pressure–volume and pressure–lattice parameter curves show near continuity in the entire pressure range. Together with the calculated high-pressure shear modulus, we find that the V sample could support a differential stress of ~ 1.58 GPa when it starts to yield with plastic deformation at ~ 36 GPa. A maximum differential stress as high as ~ 1.66 GPa can be supported by V at the high pressure of ~ 47 GPa. In addition, the bcc to rhombohedral phase transition and plastic deformation due to stress under high pressures are responsible for the development of texture.

References

[1] Wexler A and Corak W S 1952 *Phys. Rev.* **85** 85
[2] Nirmala L C and Iyakutti K 2003 *Phys. Rev. B* **67** 094509
[3] Suzuki N and Otani M 2002 *J. Phys. Condens. Matter* **14** 10869
[4] Ishizuka M, Iketani M and Endo S 2000 *Phys. Rev. B* **61** R3823
[5] Takemura K 2000 *Proceedings of the International Conference on High Pressure Science and Technology*, AIRAPT-17 (Honolulu, July 1999), edited by Manghnani M H, Nellis W J, Nicol M F (University Press, India, 2000), p. 443
[6] Suzuki N and Otani M J 2002 *J. Phys.: Condens. Matter* **14** 10869
[7] Landa A, Klepeis J, Söderlind P, Naumov I, Vitos L and Ruban A 2006 *J. Phys.: Condens. Matter* **18** 5079
[8] Ding Y, Ahuja R, Shu J, Chow P, Luo W and Mao H K 2007 *Phys. Rev. Lett.* **98** 085502
[9] Byeongchan L, Robert E R, Klepeis J E, Söderlind P and Landa A 2007 *Phys. Rev. B* **75** 180101
[10] Luo W, Ahuja R, Ding Y and Mao H K 2007 *Proc. Natl. Acad. Sci. USA* **104** 16428
[11] Koči L, Ma Y, Oganov A R, Souvatzis P and Ahuja R 2008 *Phys. Rev. B* **77** 214101
[12] Qiu S L and Marcus P M 2008 *J. Phys.: Condens. Matter* **20** 275218
[13] Verma A K and Modak P 2008 *Eurpphys. Lett.* **81** 37003
[14] Byeongchan L 2008 *Phys. Rev. B* **77** 134105
[15] Krasinikov O M, Vekilov Y K, Isaev E I and Bondarenko N G 2011 *J. Exp. Theor. Phys.* **112** 240
[16] Bondarenko N G, Vekilov Y K, Isaev E I and Krasilnikov O M 2010 *JETP Lett.* **91** 611
[17] Krasilnikov O M, Vekilov Y K, Mosyagin I Y, Isaev E I and Bondarenko N G 2012 *J. Phys.: Condens. Matter* **24** 195402
[18] Jenei Z, Liermann H P, Cynn H, Klepeis J P, Baer B J and Evans W J 2011 *Phys. Rev. B* **83** 54101
[19] Singh A K 1993 *J. Appl. Phys.* **73** 4278
[20] Singh A K and Balasingh C 1994 *J. Appl. Phys.* **75** 4956
[21] Mao H K, Xu J and Bell P M 1986 *J. Geophys. Res.* **91** 4673
[22] Liu J 2016 *Chin. Phys. B* **25** 076106
[23] Hammersley A P, Svensson S O, Hanfland M, Fitch A N and Häusermann D 1996 *High Press. Res.* **14** 235
[24] Merkel S, Wenk H R, Shu J F, Shen G Y, Gillet P, Mao H K and Hemley R J 2002 *J. Geophys. Res.* **107** 2271
[25] Duffy T S, Elert M, Furnish M D, Chau R, Holmes N and Nguyen J 2007 *AIP Con ference Proceedings* **135** 639
[26] He D W and Duffy T S 2006 *Phys. Rev. B* **73** 134106
[27] Birch F 1978 *J. Geophys. Res.* **83** 1257
[28] Ragan D D, Clarke D R and Schiferl D 1996 *Rev. Sci. Instrum.* **67** 494
[29] Shen Y R, Kumar R S, Pravica M and Nicol M F 2004 *Rev. Sci. Instrum.* **75** 4450
[30] Duffy T S, Shen G Y, Heinz D L, Shu J F, Ma Y Z, Mao H K, Hemley R J and Singh A K 1999 *Phys. Rev. B* **60** 15063
[31] Singh A K, Jain A, Liermann H P and Saxena S K 2006 *J. Phys. Chem. Solids* **67** 2197
[32] Katahara K W, Manghnani M H and Fisher E S 1979 *J. Phys. F: Met. Phys.* **9** 773
[33] Klepeis J H, Cynn H, Evans W J, Rudd R E, Yang L H, Liermann H P and Yang W G 2010 *Phys. Rev. B* **81** 134107
[34] He D W, Shieh S R and Duffy T S 2004 *Phys. Rev. B* **70** 184121
[35] Lutterotti L, Matthies S and Wenk H R 1999 *Proceeding of the Twelfth International Conference on Textures of Materials (ICOTOM-12)*, **1** 1599
[36] Lutterotti L, Matthies S and Wenk H R 1999 *IUCr: Newsletter of the CPD* **21** 14
[37] Rollett A D and Wright S I 2000 (Cambridge: Cambridge University Press) pp. 178–238
[38] Chen B, Lutker K, Raju S V, Yan J Y, Kanitpanyacharoen W, Lei J L, Yang S Z, Wenk H R, Mao H K and Williams Q 2012 *Science* **338** 1448